Fundamental Study of Momentum Exchange Impact Damper Using Pre-straining Spring Mechanism

Lovely Son, Mulyadi Bur and Meifal Rusli

Department of Mechanical Engineering, Andalas University, Indonesia.

Hiroshi Matsuhisa

Professor Emeritus, Kyoto University, 1-22-27 Hieidaira, Otsu-city, Shiga, Japan.

Keisuke Yamada and Hideo Utsuno

Department of Mechanical Engineering, Faculty of Engineering Science, Kansai University, Japan.

(Received 18 December 2014; accepted 12 October 2015)

A shock load occurred in a short time duration can lead to dangerous effect on the machine or structure. The use of conventional technique for shock vibration control by modifying the systems damping reduces the steady-state response of the system. However, this method fails to attenuate a large acceleration peak at the moment after the shock. An alternative method for reducing the maximum acceleration peak due to shock load using the principle of momentum exchange has been developed. When the shock excitation frequency is much larger in comparison with the main mass natural frequency, the passive momentum exchange impact damper(PMEID) produces good performance. However, the performance of PMEID decreases as the shock excitation frequency close to the main mass natural frequency. In this research, a simple technique to improve the performance of PMEID utilizing the pre-straining spring mechanism (PSMEID) is proposed. The dynamic model of the system with PSMEID is derived. Next, the simulation is conducted to evaluate the effectiveness of the proposed method.

1. INTRODUCTION

Shock vibration can become a serious problem in industrial and social environments.[1,2] This is not surprising, as this type of vibration induces extensive acceleration in the machine or structure during a short period of time. Consequently, adverse noise generation and large force transmission to the surroundings occur. These potentially dangerous environments could result in many effects, including damage to sensitive equipment, as well as physical human discomfort.

Solutions for such shock vibration problems have been investigated, and a number of methods have been developed to solve them. For years, simple passive shock isolators have been utilized for shock vibration control; however, space limitation and performance degradation due to the variations of excitation frequency and the system's parameters have made this technique only suitable for restricted application.

Semi-active control strategies using variable elements have been considered for improving the linear passive elements in the flexible isolator system. T. Kawashima proposed these strategies under the condition that the collision-receiving object not only has perfect plasticity, but also the colliding object has perfect elasticity.[3] T. P. Waters et al. devised a dual rate damping strategy where the damping was reduced to a lower value, whilst a shock input was applied.[4] D. F. Ledezma et al. studied the isolation of shock vibration using a variable stiffness system,[5] while application of variable damping system for shock vibration control was proposed by H. U. Oh and Y. J. Choi.[6] D. Francisco et al. studied the transient vibration control strategy using a switchable mass stiffness compound.[7]

Conventional and semi-active tuned mass damper was proposed to reduce the impact-induced vibration response.[8,9] This method was shown to reduce the steady-state response, but it failed to suppress the maximum acceleration peak from the transient response, due damper motion delay.

Some recent studies have discussed the application of active control for shock vibration problems. D. V. Balandin et al. investigated the application of pre-acting control for shock and impact isolation systems.[10] The effectiveness of the method is evaluated using a performance index defined as the maximum value of the isolated object displacement relative to the base. D. Wang et al. used the linear quadratic integral (LQI) and H_∞ control technique to control the deformation ratio between the two collision objects.[11] A gain scheduled (GS) control, which formulates when deformation changes from the elastic range to the plastic range, has also been proposed.[12]

A method for reducing the vibration system's maximum acceleration peaks from impact force using momentum exchange impact damper (MEID) was recently developed by L. Son et al.[13] Through this method, kinetic energy from the excitation load is partially transferred to the damper mass by means of a momentum exchange mechanism, thus decreasing the main

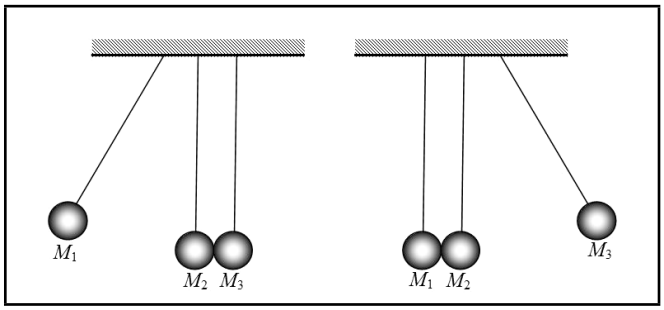

Figure 1. Newton cradle.

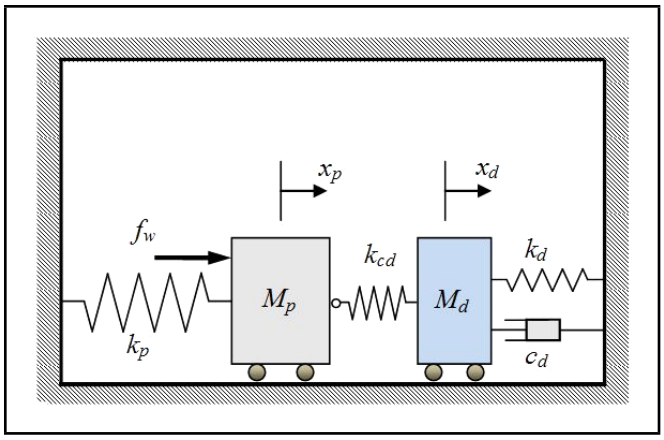

Figure 2. One DOF vibration system with PMEID.

mass vibration induced by the shock load.

The principal concept of MEID can simply be explained by the Newton cradle, which consists of the three ball system shown in Fig. 1. Part of the first ball's kinetic energy is transferred to the second upon collision. Since the second and the third balls are initially in the contact state, the second ball's kinetic energy is partly transferred to the third using momentum exchange mechanism.

The momentum exchange mechanism as explained using Newton's cradle has been used for designing the PMEID. In the PMEID application, the first ball, applying a shock load to the second, represents the shock excitation force. The second ball acts as the main body that receives the shock load; the third ball represents the impact damper system that reduces the kinetic energy using momentum exchange mechanism. Figure 2 shows one degree of freedom (DOF) vibration system using PMEID. The main mass, damper mass, main spring stiffness, and damper stiffness are represented by M_p, M_d, k_p and k_d, respectively. The shock excitation force f_w works in the main mass. The contact condition between main mass and damper mass is modelled using linear contact spring k_{cd} as shown in Fig. 2.

According to the MEID mechanism, this damper could be used to reduce the shock response of the impact induced vibration systems. Therefore, the real application of MEID is typically for reducing the shock vibration problem in machinery, such as forging machine, impact crusher, and the aircraft landing gear system.

Generally, the transfer of energy from the main mass to damper mass is maximum when time duration of the excitation force equals the contact time between the main mass and damper mass.[13] If a shock load works in a long time period, then contact force amplitude between the main mass and damper mass decreases, and a little strain energy stored is in the contact spring. Hence, the energy transfer using the momentum exchange mechanism becomes smaller, and the PMEID's performance decreases. The active momentum exchange impact damper (AMEID) that uses an actuator to generate a large contact force between the main mass and damper mass has been developed to increase the damper's performance. It is difficult, however, to find a strong enough actuator for generating a large enough contact force.[14]

Recently, a hybrid momentum exchange impact damper that uses actuators in combination with passive elements was suggested.[15] The damper, which is called an active-passive hybrid MEID (HMEID), was applied for reducing the shock responses of a landing spacecraft. This method's main disadvantages, however, is that it needs some actuators and sensors to obtain a successful damper performance.

This paper proposes a simple technique to increase momentum exchange between the main mass and damper mass using the pre-straining spring mechanism. The method is called the pre-straining spring MEID (PSMEID). By using this damper, contact force between the main mass and damper mass increases even though the shock load has long contact period. Thus, the transferred energy from the main mass to damper mass becomes larger and the acceleration of the main mass reduced significantly.

The purpose of this paper is to establish the design procedure for shock vibration control with PSMEID and to verify the capability of the proposed method. First, equations of motions illustrate how the dynamic model of one DOF vibration system with PSMEID are developed. Next, numerical simulation is conducted to investigate the damper performance for various values of system parameters. Then the optimal system parameters are calculated using time histories of the external forces working in the main mass. The comparisons between the PSMEID performances to those of the PMEID are also discussed in this paper.

2. THEORETICAL MODEL

Figure 3 shows a one degree of freedom vibration system with PSMEID. The nominal parameters for analysis examples in this paper are summarized in Table 1. The main system consists of a lumped mass M_p which is attached at a coil spring k_p as shown in Fig. 3. A half sinusoidal shock load with amplitude F_w and frequency ω_w acts on the main mass. The impact damper with mass M_d is positioned behind the main mass. The damper mass is connected to the main mass via a contact spring k_{cd}. It is assumed that the damper mass is supported by a soft spring k_d and dashpot c_d. The dashpot has a low damping coefficient for forward motion and high damping coefficient for return motion. The difference with PMEID, which uses passive elements, and PSMEID, a pre-straining spring with stiffness k_{ps}, is added between the damper mass M_d and contact

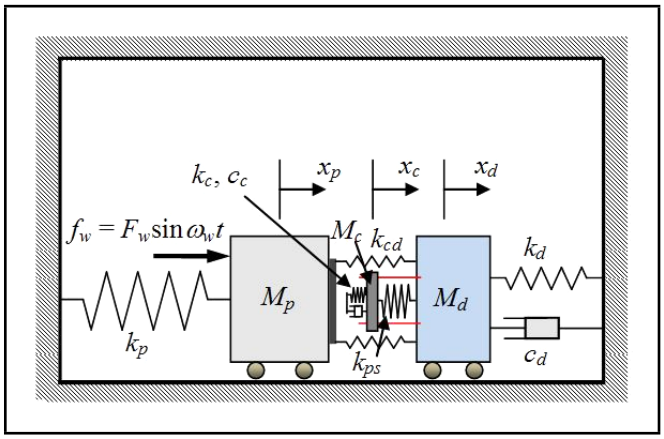

Figure 3. One DOF system with PSMEID.

Table 1. Simulation parameters.

Parameters	Value	Unit
Main mass, M_p	5.0	kg
Main spring stiffness, k_p	3.4×10^3	N/m
1st Contact spring stiffness, k_{cd}	6.5×10^3	N/m
Contact mass, m_c	5.0×10^{-3}	kg
2nd Contact spring stiffness, k_c	1.0×10^5	N/m
Contact damping, c_c	4.0	Ns/m
Pre-straining spring stiffness, k_{ps}	8.0×10^2	N/m
Damper mass, M_d	5.0×10^{-1}	kg
Damper spring stiffness, k_d	3.0×10^2	N/m
Damper damping coefficient, c_d	1.0×10^3	Ns/m
Excitation amplitude, F_w	4.0	N
Excitation frequency, ω_w	4.0	rad/s

mass M_c. The contact condition between M_c and M_p modelled using a contact stiffness k_c and contact damping c_c.

The pre-straining spring is initially compressed by the counteracting force f_t. This force causes an initial deflection x_{ps} in the pre-straining spring. An initial gap x_0 is given between the main mass and contact mass to optimize the pre-straining effect. The pre-straining spring releases at the instant after the main mass collides with the contact mass.

A simple technique to realize the pre-straining spring mechanism is by using an electromagnet device combined with the electro mechanic switch driven by a contact sensor. The magnet is attached to the damper mass. If the magnet is powered by the electric current, an electromagnetic force pulls the pre-straining spring with a constant compression force. The electro-mechanic switch system locks the pre-straining spring with the initial deflection. When the main mass collides with the contact mass, the contact sensor is on, and the electro-mechanic switch is off. As a result, the pre-straining spring is automatically releasing. Even though this mechanism could be developed for repeated shock loads, the assumption is limited for a single shock load case in this preliminary study.

The governing equations of a shock vibration system with PSMEID as shown in Fig. 3 are given as follows:

$$M_p\ddot{x}_p + k_p x_p - f_w + f_{cd} + f_c = 0; \quad (1)$$

$$M_c\ddot{x}_c - f_c + f_{ps} - f_t = 0; \quad (2)$$

$$M_d\ddot{x}_d + c_d\dot{x}_d + k_d x_d - f_{cd} - f_{ps} + f_t = 0; \quad (3)$$

It is important to note that the contact forces f_{cd} and f_c only occur during the contact period. Hence, these forces can be

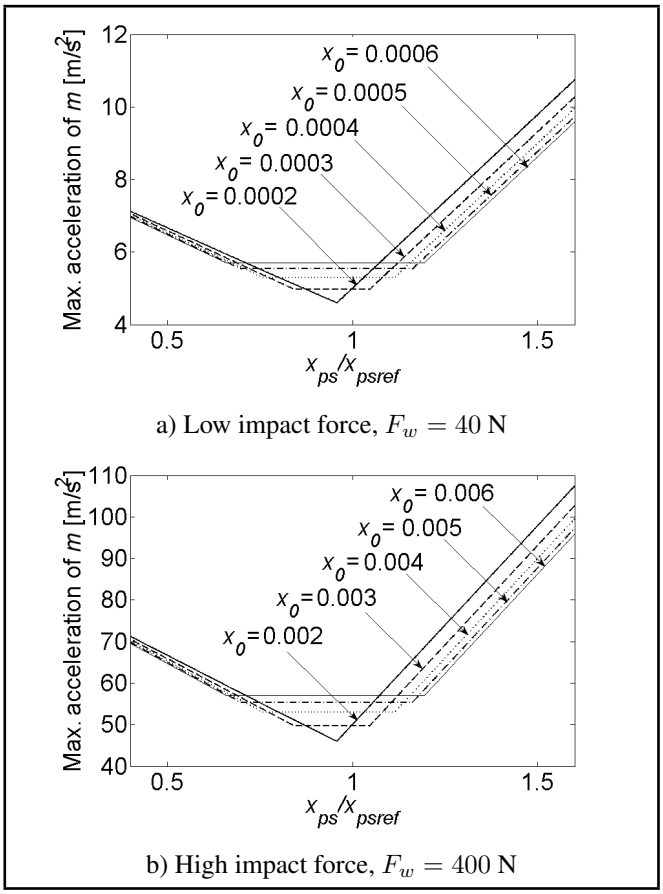

Figure 4. Variation of maximum acceleration of main mass versus x_{ps}/x_{psref}.

described as,

$$f_{cd} = \begin{cases} k_{cd}(x_p - x_d), & \text{if } x_p - x_d \geq 0 \\ 0, & \text{if } x_p - x_d < 0 \end{cases}; \quad (4)$$

and

$$f_c = \begin{cases} k_c(x_p - x_c - x_0) + c_c(\dot{x}_p - \dot{x}_c), & \text{if } x_p - x_c - x_0 \geq 0 \\ 0, & \text{if } x_p - x_c - x_0 < 0 \end{cases}. \quad (5)$$

The reaction force from pre-straining spring f_{ps} acting on M_c and M_d is proportional to the relative displacement $x_{ps} + x_c - x_d$. Therefore:

$$f_{ps} = k_{ps}(x_{ps} + x_c - x_d); \quad (6)$$

where x_{ps}, x_c and x_d are the initial compression of pre-straining spring and the displacement of M_c and M_d, respectively. The counteracting force f_t is used to counteract the pre-straining force before the main mass collides the contact spring. After collision, the counteracting force becomes zero. This relation can be expressed as

$$f_t = \begin{cases} k_{ps}x_{ps}, & \text{if } |f_c| = 0 \\ 0, & \text{if } |f_c| > 0 \end{cases}. \quad (7)$$

The simulation is conducted to investigate the performance of PSMEID, due to variations in the system's parameters. During simulation, the numerical calculation of Eqs. (1–3) are carried out in a MATLAB-Simulink computational environment, by using the fourth-order Runge-Kutta method.

3. EFFECTS OF PARAMETER VARIATIONS

In order to investigate the effects of parameter variations on the maximum acceleration response of the main mass, some important parameters must be considered.

3.1. The Effect of Pre-straining Spring Displacement (x_{ps})

Figure 4 shows variation of the main mass maximum acceleration versus x_{ps}. To simplify, non-dimensional form of pre-straining displacement x_{ps}/x_{psref} is introduced in the simulation. The reference value for pre-straining displacement x_{psref} is given by $x_{psref} = F_w/k_{ps}$. In this simulation, the pre-straining displacement is varied from $0.4 < x_{ps}/x_{psref} < 1.6$. The simulation is conducted for several values of the initial gap x_0. Other simulation parameters utilized the nominal parameter values as depicted in Table 1. Two typical cases for excitation force amplitude—low impact force ($F_w = 40$ N) and high-impact force ($F_w = 400$ N)—are used in the numerical simulation.

For a low impact case as shown in Fig. 4a, the maximum acceleration for $x_0 = 6 \times 10^{-4}$ m linearly decreases from 7 m/s^2 at $x_{ps}/x_{psref} = 0.4$ until 5.5 m/s^2 at $x_{ps}/x_{psref} = 0.65$. The maximum acceleration remains constant when $0.65 < x_{ps}/x_{psref} < 1.2$. Furthermore, the maximum acceleration increases linearly when x_{ps}/x_{psref} larger than 1.2. When the initial gap reduced to x_0 3×10^{-4} m, the constant acceleration region becomes smaller, as shown in Fig. 4a. If $x_0 = 2 \times 10^{-4}$ m, however, this constant region vanishes, and an optimum condition for x_{ps}/x_{psref} is obtained. For the high impact case, the same characteristic of the graph is obtained as shown in Fig. 4b. These results indicate that the optimum value of x_{ps} is not greatly affected by impact force amplitude. Figures 4a and 4b illustrate that an optimum value of pre-straining displacement is located near $x_{ps}/x_{psref} = 0.96$.

3.2. The Effect of Initial Gap Displacement (x_0)

Figure 5 presents the simulation results of the main mass's maximum acceleration when the initial gap x_0 and the contact stiffness k_{cd} are varied under the use of the nominal damper parameters. The simulation results present five curves with different k_{cd} values. The variations of k_{cd} are presented in the non-dimensional form, k_{cd}/k_{cdref}, as shown in Fig. 5. The reference k_{cdref} in the simulation is the same as the optimum contact stiffness for PMEID.[14] Simulations are conducted for two conditions of the excitation load: 1) low impact force ($F_w = 40$ N), and 2) high impact force($F_w = 400$ N).

Figure 5a shows the result for low impact force, while Fig. 5b depicts the result for high impact force. As can be seen from Fig. 5, the maximum acceleration for the low impact case decreases until its minimum value is at the vicinity of $x_0 = 2 \times 10^{-4}$ m, as the high impact case is near to $x_0 = 2 \times 10^{-3}$ m. Furthermore, the optimum value of x_0 is not greatly influenced by the contact stiffness k_{cd}. This phenomenon occurs because more impact energy is stored within k_c than that in k_{cd}.

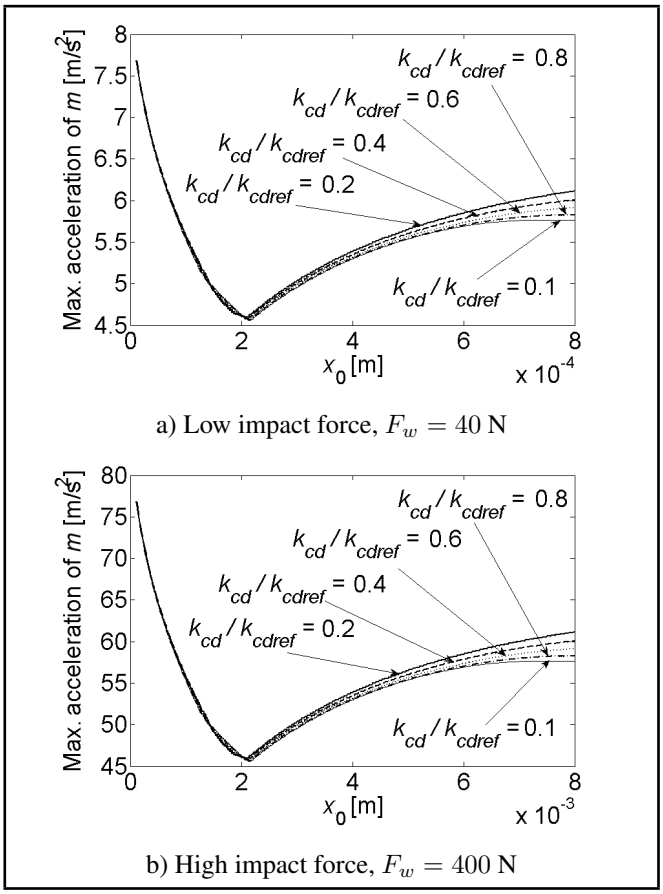

Figure 5. Variation of maximum acceleration of main mass versus x_0.

3.3. The Effect of Contact Mass (M_c) and Contact Stiffness (k_c)

Investigations of contact mass M_c and contact stiffness k_c effect to the maximum acceleration of the main mass are shown in Figs. 6a and 6b, each for low and high impact cases, respectively. Here, non-dimensional expression of contact mass M_c/M_p and contact stiffness k_c/k_{cref} are used in the simulation. The reference value $k_{cref} = 1.0 \times 10^5$ is the same as the nominal value for k_c, demonstrated in Table 1. The simulation results in Figs. 6a and 6b show that the maximum acceleration is not greatly affected by the variation of contact mass. Furthermore, increasing the contact stiffness k_c will reduce the maximum acceleration of M_p. If k_c too large, however, the damper becomes unstable. Therefore, $k_c = k_{cref}$ are used as the nominal value of the contact stiffness.

3.4. The Effect of Contact Damping (c_c)

Within the contact duration, the contact mass M_c interacts with other two masses, M_p and M_d, via the contact springs k_c and k_{ps}. Because the contact mass M_c is much smaller than M_p and M_d, the contact frequency f_c represents the motion of M_c can be expressed by

$$f_c = \frac{\omega_c}{2\pi} = \frac{1}{2\pi}\sqrt{\frac{k_e}{M_c}}; \tag{8}$$

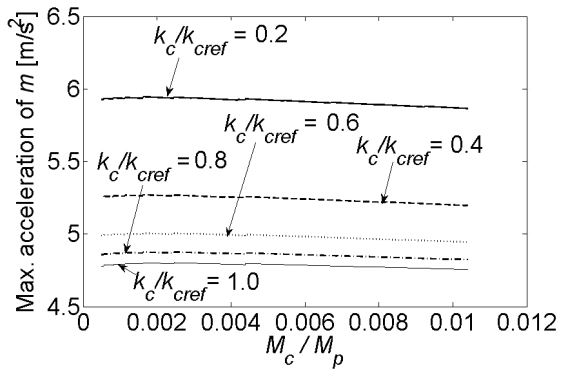

a) Low impact force, $F_w = 40$ N

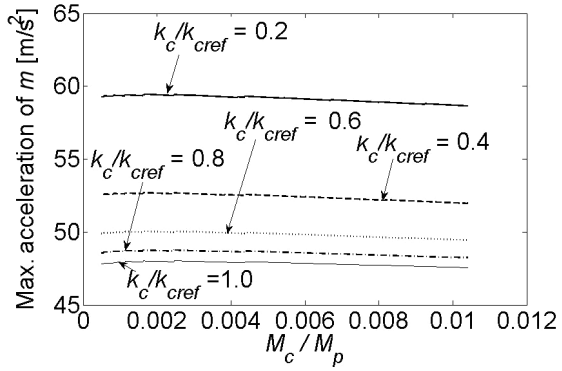

b) High impact force, $F_w = 400$ N

Figure 6. Variations of the amplitude ratio versus M_c/M_p and k_c/k_{cref}.

where the equivalent stiffness k_e is simply calculated by

$$k_e = k_c + k_{ps}. \tag{9}$$

Whenever two mechanical systems collide, some energy is dissipated in the high stress region of contact.[16] The level of dissipated energy during contact between M_p and M_c can be expressed by a contact damping ratio ζ_c

$$\zeta_c = \frac{c_c}{2M_c\omega_c}; \tag{10}$$

where c_c is the viscous contact damping between M_p and M_c. Figure 7 shows several acceleration responses of the main mass at the moment after contact. The responses are calculated using several values of contact damping ratio ζ_c. For low damping ratio ($\zeta_c = 0.1$), the acceleration response has a large amplitude of oscillation. When the damping ratio is increased, the acceleration response becomes smooth, and the oscillation disappears when $\zeta_c = 1$, as shown in Fig. 7.

3.5. The Effect of Pre-straining Stiffness (k_{ps})

The amount of momentum transferred to damper mass depends on the stiffness of pre-straining spring k_{ps}. As a result, the selection of k_{ps} is important for obtaining the minimum acceleration and displacement response of M_p. Figures 8a and 8b show the results of maximum acceleration and main mass displacement when k_{ps} is varied. The optimum parameters of x_0 and x_{ps} obtained in previous chapter are used in the simulation.

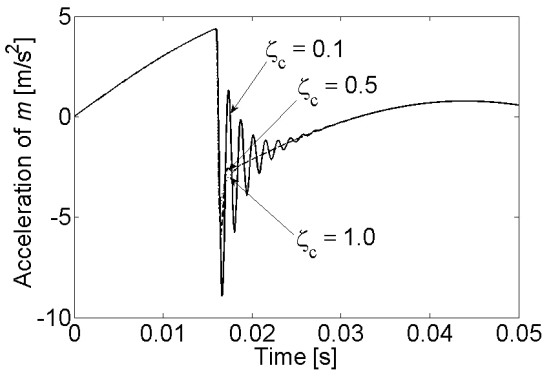

Figure 7. Acceleration of M_p for several values of damping ratio.

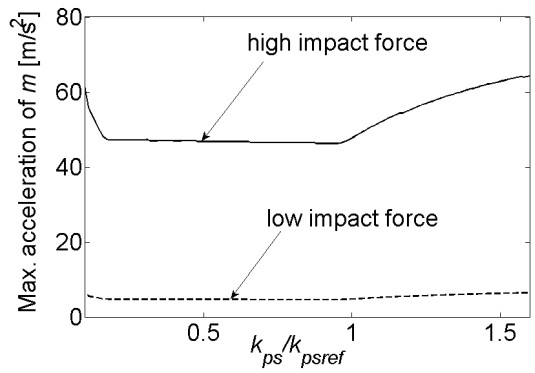

a) Maximum acceleration of m

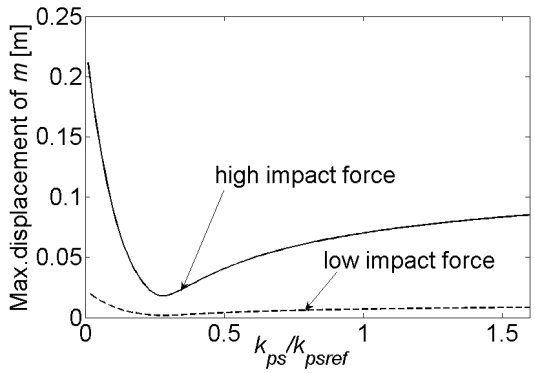

b) Maximum displacement of m

Figure 8. Variation of maximum acceleration and displacement versus k_{ps}/k_{psref}.

The simulations are conducted for low and high impact force conditions. The pre-straining stiffness k_{ps} is normalized by dividing it by $k_{psref} = M_d\omega_w$. As observed from Fig. 8a, the maximum acceleration of M_p is not greatly affected by variation of the pre-straining spring stiffness k_{ps} for the low impact case. In the case of high impact force, however, the optimum range of k_{ps} is located at $0.2 < k_{ps}/k_{psref} < 0.9$. Meanwhile, the maximum displacement of M_p for low and high impact cases, as shown in Fig. 8b, greatly depend on the variations of pre-straining spring stiffness. Figure 8b also shows that the main mass maximum displacement has a minimum value at the vicinity of $k_{ps}/k_{psref} = 0.25$.

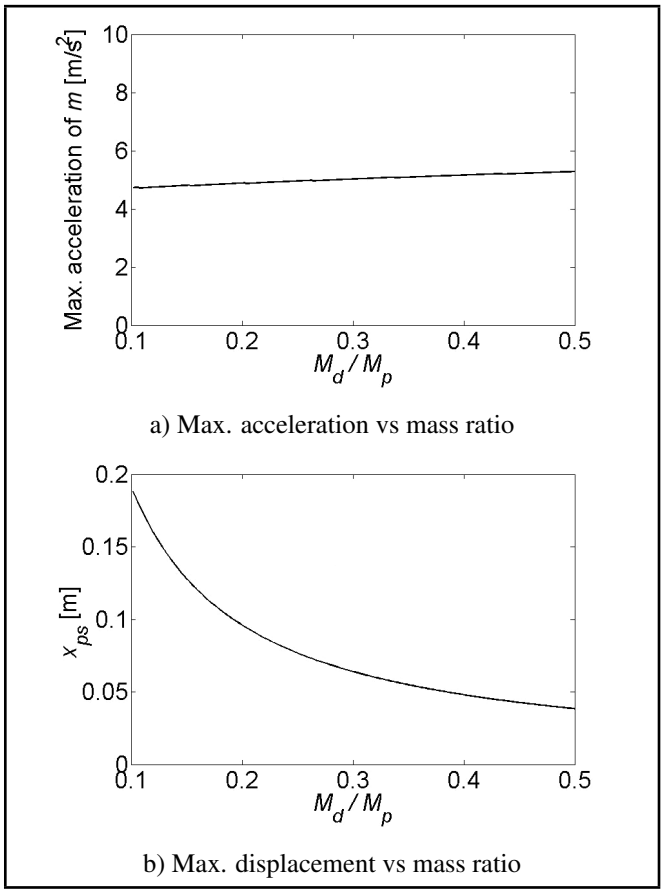

Figure 9. Optimum condition of PSMEID performance evaluated with variation of M_d/M_p.

3.6. The Effect of Damper Mass (M_d)

The results of main mass maximum acceleration and related initial displacement of pre-straining spring plotted against the damper mass variations (M_d/M_p) are shown Fig. 9. Here, the optimal parameters obtained in previous chapter are used in the simulation. The simulation is conducted for a low impact case ($F_w = 40$ N), and its results, shown in Fig. 9a, indicate that the maximum acceleration of the main mass is not greatly affected by the damper mass variation. For small values of damper mass, however, the initial displacement of the pre-straining spring should be large for generating a large contact force as seen in Fig. 9b.

The results from Fig. 9 demonstrate that the main mass acceleration peak could be reduced using small values of damper mass. A negative effect, however, is that the maximum transmitted force, from the damper to ground, increases due to large damper mass displacement.

3.7. Contact Time Analysis

Momentum exchange between two oscillators during collision is greatly dependent upon the contact time duration.[16] This condition is also met in the momentum exchange impact damper. Therefore, the contact time duration between main mass and damper mass directly affects the amount of transferred energy between them.

When a large amount of energy is transferred from M_p to M_d, the energy stored in the spring of the main mass is small.

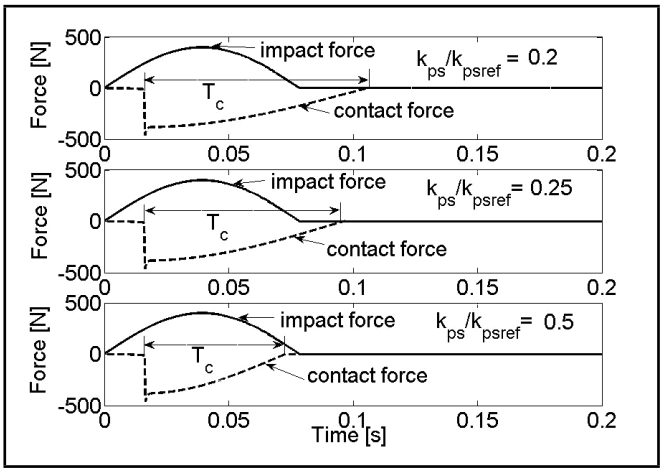

Figure 10. External forces time histories for three values of k_{ps}.

As the consequence, the displacement of the main mass decreases. According to the results obtained from Fig. 9b, the main mass displacement depends largely on the value of pre-straining spring stiffness k_{ps}. To investigate the relation between k_{ps} and the contact time duration, three conditions of the pre-straining spring stiffness are studied: $k_{ps}/k_{psref} = 0.2$, $k_{ps}/k_{psref} = 0.25$, and $k_{ps}/k_{psref} = 0.5$. The simulations are conducted for high impact force ($F_w = 400$ N). The optimal parameters previously obtained are utilized in the simulation.

Figure 10 shows the results of external force time histories acting in the main mass. The impact force (f_w) is a half-sinusoidal function, with amplitude and frequency F_w and ω_w, respectively. The resulting contact force in the main mass ($f_c + f_{cd}$) is induced by the contact spring k_c and k_{cd}. As can be seen in Fig. 10, the maximum values of contact force are almost constant for all pre-straining spring stiffness values. Meanwhile, the contact time between main mass and impact damper are changed due to variation of the pre-straining spring stiffness. Here, the contact time (T_c) is measured as time duration when the main mass initially collides the contact spring until the contact between them is losses. The results in Fig. 10 indicate that contact time duration is highly dependent on the pre-straining spring stiffness.

If we neglect the effect of contact mass m_c and contact stiffness k_c, then the impact damper system seen in Fig. 3 can be assumed as collision between two oscillators.[16] In this collision, the contact time between the main mass and impact damper is simply calculated using the equation of motion for difference displacement. For weak impact condition, the contact duration increases with impact strength β according to

$$T_c = \frac{\pi\beta}{\omega_{rr}\sqrt{2}}; \tag{11}$$

where ω_{rr} is the interaction frequency between M_p and M_d, as given by

$$\omega_{rr} = \sqrt{\frac{k_0 + k_{ps}}{M_0}}. \tag{12}$$

If the damping of the main mass and impact damper are neglected, the interaction mass and stiffness can be calculated

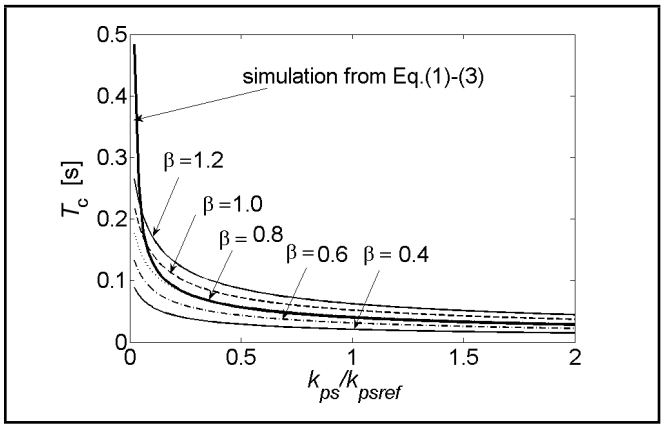

Figure 11. Comparisons of contact time.

by[16]

$$M_0 = \frac{M_p \cdot M_d}{M_p + M_d} \quad \text{and} \quad k_0 = \frac{k_p \cdot k_d}{k_p + k_d}. \tag{13}$$

Figure 11 shows the comparison of contact time (T_c) calculated by simulation of Eqs. (1–3) and those calculated using Eq. (11) for several values of impact strength (β). The contact periods increase when the impact strength increases from 0.4 to 1.2. The impact strengths are greatly dependent on the ratio between kinetic energy and strain energy of the vibration system at contact.[16] For impact strength value ($\beta = 0.8$), the contact time calculated from the simulation of Eqs. (1–3) is similar to those calculated using Eq. (11). For small values of k_{ps}, however, these two methods provide different values of contact time. This variation might be due to the assumption that k_{cd}, M_c and k_c are neglected in the calculation of Eq. (11), whilst for the small values of k_{ps}, these factors become dominant for calculation of contact time.

3.8. Simple Calculation of x_0, x_{ps} and k_{ps} Optimum Values Using External Force Time History

The maximum acceleration peak of the main mass under shock load occurs during the contact period. At this period, acceleration of M_p is proportional to the resultant external forces experienced by the main mass. Figure 12 shows the external force's time histories acting on the main mass for low and high impact forces, corresponding to the optimal PSMEID parameters. The contact force is zero before collision between the main mass and contact spring occurs. After the main mass collides the contact spring, the contact force increases drastically. This condition is starting at $t = T_w/10$, where $T_w/2$ is the excitation period of the external force f_w.

The equation of motion of the main mass before collides the contact spring k_c can be expressed by

$$M_p \ddot{x}_p + k_p x_p = f_w. \tag{14}$$

If the excitation force is assumed as a half-sinusoidal function with amplitude F_w and frequency ω_w then the main mass displacement for zero initial conditions can be expressed by

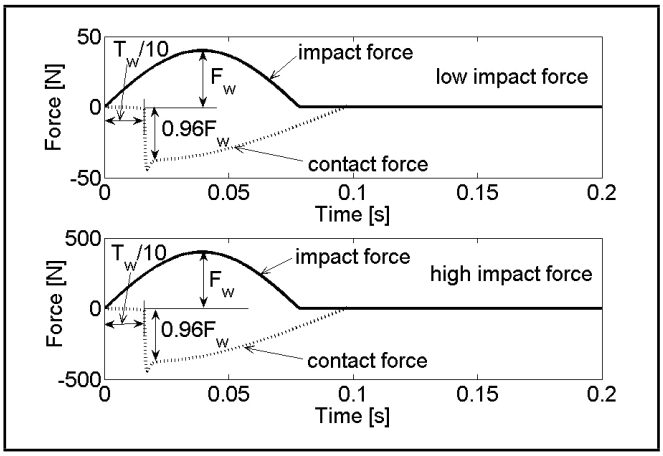

Figure 12. Contact force time history at optimum parameter's condition.

$$x_p(t) = \frac{\frac{F_w}{k_p}}{1 - \left(\frac{\omega_w}{\omega_n}\right)^2} \left(\sin \omega_w t - \frac{\omega_w}{\omega_n} \sin \omega_n t\right); \tag{15}$$

where ω_n is the natural frequency of the main mass. The optimum value of x_0 is the main mass displacement at $t = T_w/10$. Substituting $t = T_w/10$ into Eq. (15) results in

$$(x_0)_{\text{optimum}} = x_p\left(\frac{T_w}{10}\right) = \frac{\frac{F_w}{k_p}}{1 - \left(\frac{\omega_w}{\omega_n}\right)^2} \left[\sin\left(\frac{2\pi}{10}\right) - \frac{\omega_w}{\omega_n} \sin\left(\frac{2\pi\omega_n}{10\omega_w}\right)\right]. \tag{16}$$

Investigation of the external force time histories presented in Fig. 12 shows that the minimum acceleration peak of the main mass occurs when the maximum peak of the contact force (not involved the overshoot) is equal to $0.96F_w$. This relation can be expressed mathematically by

$$\max(f_{cd} + f_c) = 0.96F_w. \tag{17}$$

It should be noted that the overshoot in Fig. 12 occurs due to vibration of the contact mass M_c. Considering the results obtained from Fig. 5, the main mass minimum acceleration is not affected by k_{cd}. Therefore, Eq. (17) can be simplified as

$$\max(f_c) = 0.96F_w. \tag{18}$$

The maximum values of f_c in Eq. (18) are occuring at the moment after the main mass collides the contact spring k_c. At this time the counteracting force f_t becomes zero, and the maximum contact force becomes $f_c = k_{ps}x_{ps}$. Thus, Eq. (18) can be written as

$$(x_{ps})_{\text{optimum}} = 0.96\frac{F_w}{k_{ps}} = 0.96x_{psref}. \tag{19}$$

The external force time histories presented in Fig. 12 show that the optimal condition for transferring the momentum from the main mass to the damper occurs when the contact time is

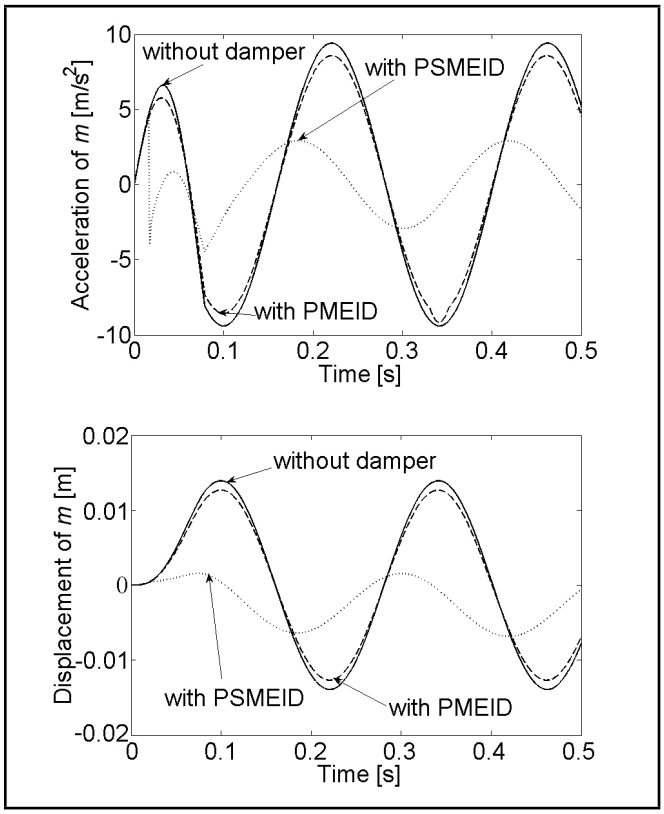

Figure 13. Acceleration and displacement of mass m.

the same as the excitation time ($T_c = T_w/2$). This condition complies with the results obtained from the three-body impact system.[13] This relation can be expressed mathematically by

$$T_c = \frac{T_w}{2} \quad \text{or} \quad T_c = \frac{\pi}{\omega_w}. \tag{20}$$

By eliminating T_c in Eq. (20) by using Eq. (11), then the optimal condition for pre-straining spring can be calculated by

$$(k_{ps})_{\text{optimum}} = \frac{M_0 \omega_w^2 \beta^2}{2} - k_0; \tag{21}$$

where M_0 and k_0 are given in Eq. (13). Substitution of the nominal systems parameters in Table 1 into Eq. (21), provides a non-dimensional form of the optimal k_{ps} as given by:

$$\left(\frac{k_{ps}}{k_{psref}}\right)_{\text{optimum}} = 0.253. \tag{22}$$

The optimal k_{ps} calculated using Eq. (22) is close to that obtained from the simulation as shown in $k_{ps}/k_{psref} = 0.25$ in Fig. 8b.

3.9. Comparison Performance of PSMEID and PMEID

The simulation is conducted to highlight the effectiveness of momentum exchange impact damper performance using pre-straining spring mechanism. Time history of the main mass acceleration and displacement using PSMEID are then compared with those obtained without damper and using PMEID. The simulation results are shown in Fig. 13. The excitation force amplitude and frequency used in this simulation are

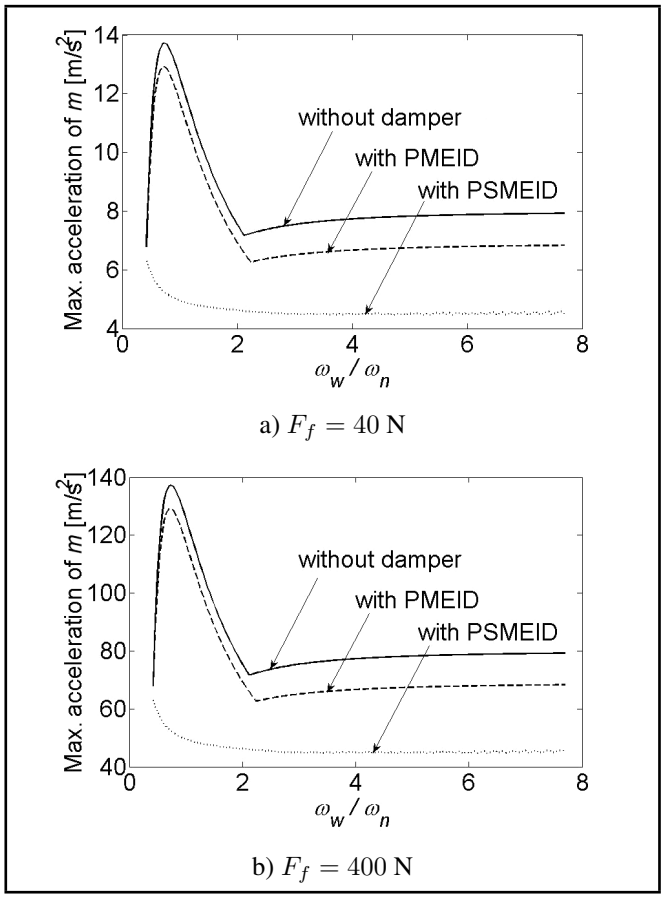

Figure 14. Maximum acceleration of m with variation of ω_w.

$F_w = 40$ N and $\omega_w = 40$ rad/s. The damping ratio ζ_c is set to 1 and the optimum parameters obtained in the previous chapter are used in the simulation.

The simulation results of impact damper performance evaluated with variation of the shock excitation frequency are presented in Fig. 14. Figure 14 also shows the maximum acceleration of M_p obtained using three cases: without damper, with PMEID, and with PSMEID. The simulation results presented in Fig. 14 indicate that the maximum acceleration peak of the main mass obtained using PSMEID is smaller than those obtained using PMEID in the whole impact frequency range. Furthermore, PMEID performance decreases when the impact frequency close to the main mass natural frequency ($\omega_w/\omega_n \approx 1$); however, this phenomenon is not occuring in PSMEID.

4. CONCLUSIONS

This paper proposes a method to improve the momentum exchange impact damper performance for attenuating shock vibration using pre-straining spring mechanism (PSMEID). The proposed damper can significantly reduce the maximum acceleration peak and displacement of the main mass. The effectiveness of the system is evaluated by simulations. The results are summarized as follows:

1. The initial gap x_0, the initial pre-straining spring displacement x_{ps} and stiffness k_{ps}, are important parameters

for designing the momentum exchange impact damper using pre-straining spring mechanism.

2. Simple calculation using external force's time histories can be used to obtain the optimal values of x_0, x_{ps} and k_{ps}.

3. The performance of PSMEID increases when the value of the contact stiffness k_c increases; however, when k_c is too large, the system becomes unstable.

4. The value of contact mass M_c does not significantly affect the performance of PSMEID.

5. The maximum acceleration of main mass could be reduced using small value of impact damper mass M_d. When the damper mass is very small, however, the transmitted force from the damper to the ground becomes large.

6. As opposed to PMEID, whose performance decreases when excitation frequency is close to main mass natural frequency, PSMEID performance is not greatly affected by main mass natural frequency.

ACKNOWLEDGEMENTS

The first author gratefully acknowledges the Andalas University International Publication Acceleration Grant No. 10/UN.16/PL/API/2014 for funding this work.

REFERENCES

[1] Tanaka N. and Kikushima, Y. A study of a servo damper with preview action (an optimal design for impact vibration control), *JSME International Journal*, **32** (2), 215–222, (1989). https://dx.doi.org/10.1299/jsmec1988.32.215

[2] Son L., Kawachi M., Matsuhisa H., and Utsuno, H. Reducing floor impact vibration and sound using a momentum exchange impact damper, *Journal of System Design and Dynamics*, **1** (1), 14–26, (2007). https://dx.doi.org/10.1299/jsdd.1.14

[3] Kawashima, T. Consideration of optimal input on semi-active shock control system, *Journal of System Design and Dynamics*, **2** (1), 127–138, (2008). https://dx.doi.org/10.1299/jsdd.2.127

[4] Waters T. P., Hyun Y., and Brennan M. J. The effect of dual-rate suspension damping on vehicle response to transient road inputs, *Journal of Vibration and Acoustic*, **131** (1), (2009). https://dx.doi.org/10.1115/1.2980370

[5] Ledezma D. F., Fergusson N. S., and Brennan M. J. Shock isolation using an isolator with switchable stiffness, *Journal of Sound and Vibration*, **330** (5), 868–882, (2011). https://dx.doi.org/10.1016/j.jsv.2010.09.016

[6] Oh H. U. and Choi Y. J. Performance investigation of variable damping shock absorber combined with conventional semi-active vibration control logics, *Aerospace Science and Technology*, **29** (1), 1–6, (2013) https://dx.doi.org/10.1016/j.ast.2013.01.001

[7] Francisco D., Ferguson N. S., and Zamarripa A. S. Mathematical modeling of a transient vibration control strategy using a switchable mass stiffness compound, *Journal of Shock and Vibration*, 1–10, (2014). https://dx.doi.org/10.1155/2014/565181

[8] Setareh M. and Hanson R. D. Tuned mass damper to control floor vibrations from humans, *ASCE Journal of Structural Engineering*, **118** (3), 741–762, (1992). https://dx.doi.org/10.1061/(asce)0733-9445(1992)118:3(741)

[9] Setareh M., Ritchey J. K., Murray T. M., Koo J. H., and Ahmadian M. Semiactive tuned mass damper for floor vibration control, *Journal of Structural Engineering*, **133** (2), 242–250, (2007). https://dx.doi.org/10.1061/(asce)0733-9445(2007)133:2(242)

[10] Balandin D. V., Bolotnik N. N., and Pilkey W. D. Preacting control for shock and impact isolation systems, *Journal of Shock and Vibration*, **12** (1), 49–65, (2005). https://dx.doi.org/10.1155/2005/578381

[11] Wang D., Nishimura H., and Shimogo T. Active control of shock (application of LQI control and H_∞ control), *Transactions of JSME, Ser. C* (in Japanese), **71** (704), 1223–1230, (2005). https://dx.doi.org/10.1299/kikaic.71.1223

[12] Wang D., Nishimura H., and Shimogo T. Active control of shock by gain scheduling, *Journal of Sound and Vibration*, **308** (3–5), 647–659, (2007). https://dx.doi.org/10.1016/j.jsv.2007.03.080

[13] Son L., Matsuhisa H., and Utsuno H. Energy transfer in a three-body momentum exchange impact damper, *Journal of System Design and Dynamics*, **2** (1), 425–441, (2008). https://dx.doi.org/10.1299/jsdd.2.425

[14] Son L., Hara S., Yamada K., and Matsuhisa H. Experiment of shock vibration control using active momentum exchange impact damper, *Journal of Vibration and Control*, **16** (1), 49–64, (2009). https://dx.doi.org/10.1177/1077546309102675

[15] Kushida Y., Hara S., Otsuki M., Yamada Y., Hashimoto T., and Kubota, T. Robust Landing gear system based on a hybrid momentum exchange impact damper, *Journal Of Guidance, Control, And Dynamics*, **36** (3), 776–789, (2013). https://dx.doi.org/10.2514/1.58373

[16] Pinnington R. J. Collision dynamics of two adjacent oscillators, *Journal of Sound and Vibration*, **268** (2), 343–360, (2003). https://dx.doi.org/10.1016/s0022-460x(03)00411-5